A&A 394, 835–849 (2002)
DOI: 10.1051/0004-6361:20021235

Astronomy & Astrophysics

Exploring the spectral properties of faint hard X-ray sources with *XMM–Newton*

E. Piconcelli[1,2], M. Cappi[1], L. Bassani[1], F. Fiore[3], G. Di Cocco[1], and J. B. Stephen[1]

[1] IASF/CNR, via Piero Gobetti 101, 40129 Bologna, Italy
[2] Dipartimento di Astronomia, Università di Bologna, via Ranzani 1, 40127 Bologna, Italy
[3] Osservatorio Astronomico di Roma, Via Frascati 33, 00044 Monteporzio, Italy

Received 15 March 2002 / Accepted 26 August 2002

Abstract. We present a spectroscopic study of 41 hard X-ray sources detected serendipitously with high significance ($>5\sigma$ in the 2–10 keV band) in seven *EPIC* performance/verification phase observations. The large collecting area of *EPIC* allows us to explore the spectral properties of these faint hard X-ray sources with $2 < F_{2-10} < 80 \times 10^{-14}$ erg cm^{-2} s^{-1} even though the length of the exposures are modest (~20 ks). Optical identifications are available for 21 sources of our sample. Using a simple power law plus Galactic absorption model we find an average value of the photon index $\Gamma \sim 1.6$–1.7, broadly consistent with recent measurements made at similar fluxes with *ASCA* and with *Chandra* stacked spectral analyses. We find that 31 out of 41 sources are well fitted by this simple model and only eight sources require absorption in excess of the Galactic value. Interestingly enough, one third of these absorbed sources are broad line objects, though with moderate column densities. Two sources in the sample are X-ray bright optically quiet galaxies and show flat X-ray spectra. Comparing our observational results with those expected from standard synthesis models of the cosmic X-ray background (CXB) we find a fraction of unabsorbed to absorbed sources larger than predicted by theoretical models at our completeness limit of $F_{2-10} \sim 5 \times 10^{-14}$ erg cm^{-2} s^{-1}. The results presented here illustrate well how wide-angle surveys performed with *EPIC* on board *XMM-Newton* allow population studies of interesting and unusual sources to be made as well as enabling constraints to be placed on some input parameters for synthesis models of the CXB.

Key words. galaxies: active – X–rays: galaxies – X–rays: diffuse background

1. Introduction

It is now widely accepted that the bulk of the Cosmic X-ray background (CXB) in the range 0.1–10 keV is the result of the integrated emission of unresolved sources over cosmic time (Giacconi et al. 2001). Recent extremely deep surveys by *Chandra* (Tozzi et al. 2001; Brandt et al. 2001a) and *XMM-Newton* (Hasinger et al. 2001), have resolved up to ~75–90% of the CXB into discrete sources, down to a limiting 2–10 keV flux of $\sim 10^{-16}$ erg cm^{-2} s^{-1}. On-going follow-up optical identification programs suggest that most of these sources are AGNs, while a sizeable fraction of the rest are optically faint ($I > 24$) objects (~30%), likely to be highly obscured AGNs (Alexander et al. 2001) or luminous bulge-dominated galaxies (Barger et al. 2001; Cowie et al. 2001). Large area surveys (e.g. from *ASCA* and *BeppoSAX*; Akiyama et al. 2000; Della Ceca et al. 1999; Giommi et al. 2000), limited to higher fluxes but providing a larger number of sources, confirm the above results. At a flux limit of $\sim 5 \times 10^{-14}$ erg cm^{-2} s^{-1} in the range 5–10 keV, the bulk of the sources are broad line AGNs, while most of the others are classified as Seyfert 1.8–2 galaxies and optically "red" quasars (La Franca et al. 2000). Surprisingly, *Chandra* serendipitously discovered that also some normal galaxies, without evidence for any activity (i.e. AGN and/or starburst) in the optical band, are X-ray loud (Fiore et al. 2000).

To date very few X-ray spectra of such faint sources are reported in the literature (but see pioneering results from Vignali et al. 2000; Sakano et al. 1998 and Crawford et al. 2001). Such spectral information is crucial in order to accurately determine source-by-source the amount of absorption, the spectral shape and the presence of reprocessed features (see e.g. Yaqoob 2000). These can also be used as input parameters for the synthesis models of the CXB in order to evaluate the contribution of the various AGN types and constrain their evolution (Comastri et al. 2001; Gilli et al. 2001). Important questions are still unanswered, such as the relationship between optical identification and X-ray characteristics as well as the role of absorption in the different types of active galaxies (Salvati & Maiolino 2000; Pappa et al. 2001a). There is growing evidence that not only narrow line but also broad line AGNs suffer from intrinsic absorption (Risaliti et al. 2000), which is present both in radio-quiet (Gallagher et al. 2000;

Send offprint requests to: E. Piconcelli,
e-mail: piconcel@tesre.bo.cnr.it

Brandt et al. 2001b; Maloney & Reynolds 2001; Collinge & Brandt 2000) and in radio-loud objects (Cappi et al. 1997; Yuan et al. 2000; Sambruna et al. 1999) at all redshifts. These obscured sources show hard spectral indices which match well with the CXB slope in the hard X-ray band (∼1.4, e.g. Marshall et al. 1980). Moreover doubts are emerging about the existence of the long sought after high luminosity type 2 AGNs (Halpern et al. 1999), the so-called QSO 2s, which should play a significant (and perhaps a major) role in the production of the hard CXB (Fabian & Iwasawa 1999): from recent deep observations only two cases have been reported (Norman et al. 2001; Stern et al. 2001). It would appear to be difficult to discover a large number of distant Compton-thick QSOs with present X-ray observatories (Fabian et al. 2001).

Based on the above arguments, we have started an extensive program with *XMM-Newton* aimed at studying the brightest (in the hard X-ray band) sources serendipitously detected in a number of fields with moderate exposure (∼20 ks). This work has been designed to complement at an intermediate flux level ($\sim 10^{-14}$ erg cm^{-2} s^{-1}) the X-ray population studies made by very deep pencil-beam observations. On account of its good positional accuracy (∼6 arcsec error radius) and its unprecedented sensitivity in the 2–10 keV band, the *XMM-Newton* satellite is currently the most appropriate telescope with which to pursue such a study.

2. *XMM−Newton* observations

2.1. Data reduction

The *XMM-Newton* observatory was launched on December 10th 1999 and was placed in a 48 hour orbit (Jansen et al. 2001). *EPIC* (*European Photon Imaging Cameras*) on-board *XMM-Newton* consists of two *MOS* CCD front-illuminated arrays (Turner et al. 2001) and one *PN* CCD back-illuminated array (Struder et al. 2001) for X-ray imaging and spectroscopy in the range ∼0.1–10 keV. Each camera is located in the focal plane of one of three X-ray grazing incidence telescopes and provides a 30 arcmin diameter field of view. *EPIC* is equipped with a filter wheel which carries three different blocking filters, i.e. Thin (40 nm Al), Medium (80 nm Al) and Thick (200 nm Al), optimised for different investigations.

In the present study we investigate the *EPIC* fields of seven observations performed during the performance/verification phase. These fields are listed in Table 1 together with their observational details. They cover in total an area of ∼1.4 deg^2 of the sky and they all have $b \geq 30$ deg so that we can exclude heavy contamination from Galactic sources and high Galactic column densities along the line of sight. We are able to reach 4–5 arcsec absolute pointing accuracy reconstruction for the boresight instruments using the Attitude History Files (AHFs) available for all datasets, as demonstrated by the *EPIC* calibrations (for more details see `http://xmm.vilspa.esa.es/users/calib_top.html`).

The raw *EPIC* observation data files (ODFs) are reduced and analysed using the standard Science Analysis System (*SAS*) software package (version 5.0, released in 2000, December 15th; Gondoin 2001). We use the EPCHAIN and EMCHAIN tasks for the pipeline processing of the ODFs to generate the corresponding event files. These tasks also allow dead and hot pixels to be removed. On each event file we then apply an exposure time correction in order to exclude intervals contaminated by soft proton flares: we extract background lightcurves at energy >10 keV to identify and remove periods of high count rates (typically 0.2 cts/s). The resulting clean integration times for each *EPIC* camera are listed in Table 1. We select pixel patterns ≤12 and =0 for *MOS* and *PN* events, respectively, in order to filter out cosmic-ray tracks and/or spurious noise events not created by X-rays. We use the XMMSELECT task to filter data and to generate lightcurves, images and spectra. All our images are binned to obtain a pixel-size of 4.4 × 4.4 arcsec.

2.2. Sample creation

We have created a 2–10 keV *PN* image of all but one (IRAS 13349+2438) of the fields listed in Table 1 which have then been used to detect hard X-ray serendipitous sources. The *PN* observation of IRAS 13349+2438 was carried out in small window mode (Studer et al. 2001) and so we have used a 2–10 keV *MOS1* image of this field. We investigate in the 2–10 keV range because to date it is the nearest X-ray spectroscopically accessible band to the CXB νF_ν peak at ∼30 keV. The main reason for which we choose the *PN* camera to perform such a survey is its greater effective area with respect to the *MOS* (in particular in the hard band it is a factor ∼2.5 times at 8 keV), which enables us to be more accurate in the detection of faint hard X-ray sources.

In the following we briefly summarize our detection procedure. For each 2–10 keV image we generate an exposure map containing information about filter transmission and spatial quantum efficiency which has been used by other *SAS* tasks of the detection chain. The area of the image where source searching is performed is marked by a detection mask created by the EMASK task. We run the EBOXDETECT task, the standard *SAS* sliding box cell detection algorithm, with local background subtraction (i.e. "local mode") in order to have a list of candidate sources. This list is given as input to the ESPLINEMAP task to produce a smooth background map. This background map is then used in a second EBOXDETECT procedure (i.e. "map mode"). We choose $L = -\ln(P) = 15$ as the minimum detection likelihood value corresponding to a probability of Poissonian random fluctuations of the counts in the detection cell of $P = 3.0 \times 10^{-7}$ (roughly ∼5σ). EBOXDETECT generates a list of selected sources with their centroid coordinates (x, y). Finally we include in our sample only those sources detected with at least 35 net counts in a 5×5 pixel box centered on (x, y). These counts are raw and they must be corrected for both the energy encircled fraction (EEF) and the vignetting factor: in this way our selection criterion (i.e. 35 counts) corresponds, for example, to a corrected final flux of $F_{2-10} \sim 2.3 \times 10^{-14}$ erg cm^{-2} s^{-1} for an on-axis source and to $F_{2-10} \sim 5 \times 10^{-14}$ erg cm^{-2} s^{-1} for a 10 arcmin off-axis source in our shortest *PN* exposure (i.e. 15 ks, see Table 1). As the *PN* and

Table 1. Journal of the *XMM-Newton* observations.

Field	RA	Dec	Orbit	Date	Exposure (s)			Filter
					PN	M1	M2	PN M1 M2
PKS 0312−770	03 11 55.0	−76 51 52	057	2000-03-31	26 000	25 000	24 000	Tc Tc Tc
MS 1229.2+6430	12 31 32.0	+64 14 21	082	2000-05-20	22 900	18 600	22 900	Th Th Th
IRAS 13349+2438	13 37 19.0	+24 23 03	097	2000-06-20	–	41 300	38 600	– Me Th
Abell 2690	00 00 30.0	−25 07 30	088	2000-06-01	21 000	16 600	15 300	Me Me Me
MS 0737.9+744	07 44 04.5	+74 33 49	063	2000-04-12	15 000	17 800	26 100	Th Th Th
Markarian 205	12 21 44.0	+75 18 37	075	2000-05-07	17 000	–	14 800	Me – Me
Abell 1835	14 01 02.0	+02 52 41	101	2000-06-27	22 900	23 700	26 400	Th Th Th

Optical blocking filters used during observations: Th = thin, Me = medium and Tc = thick.

MOS FOVs differ slightly we also perform the detection procedure described above on the *MOS* images in order to detect those sources which lie in the gaps between the *PN* chips or out of the *PN* FOV. The selection criterion remains the same, except for the fact that in this case we accept only sources having at least 20 net counts in a 5×5 pixel box centered on (x, y). In this way we include a further 4 sources (2 in the gaps and 2 out of the FOV) which were previously undetected. In total we obtain a sample of 41 hard X-ray selected serendipitous sources. They are listed in Table 2.

2.3. Spectral analysis

All spectra are extracted in the 0.3–10 keV band where *EPIC* is best calibrated. The corresponding background regions are extracted from offset positions close to the sources, in source-free regions and with the same radii of the source regions (i.e. 35 arcsec). For a few cases, the extraction radius was reduced due to the presence of another nearby source or of the CCD gaps. The latest response matrices (released in July 2001) for the corresponding filters are used for the analysis. All our spectra are also corrected for vignetting. It is worth noting, however, that for off-axis angles >10 arcmin the vignetting function is energy independent below ∼5 keV for all *EPIC* detectors (with a ratio between off-axis and on-axis counts of ∼0.6, Gondoin et al. 2000): since ∼80% of our sources (32 out of 41) are detected within 10 arcmin off-axis the spectral correction for vignetting is only significant for a small number of sources. Therefore we expect little or almost negligible contamination in the determination of the spectral parameters during our analysis. For each source of the sample, we perform a combined spectral fitting using the data of both *MOS* and *PN* detectors, whenever both datasets are available. Before spectral fitting, all spectra are binned with a minimum of 20 counts per bin in order to be able to apply the χ^2 minimization technique. In the cases of relatively poor statistics (i.e. <400 final counts in the 0.3–10 keV band) the minimun number of counts per bin is set to 15 and we apply the Gehrels weighting method (Gehrels 1986) in our analysis. However heavy binning of data with poor statistics can result in a loss of spectral information, so for a worthwhile comparison we also use the Cash statistic (Cash 1979) to estimate the fit parameters and their errors in the *PN* data analysis of those sources characterized by only few photons. This is a maximum likelihood method which allows the use of unbinned data but it assumes that the counts in a given channel follow a Poisson distribution, so that it cannot be applied to background-subtracted data. Hence before performing spectral modelling we accurately parameterize the background in a large source-free region with a model consisting of a broken power law plus Gaussian lines as suggested in Lumb et al. (2002). Then we include this model for the background (fixing the values of the parameters and rescaling the normalizations to the area of the extraction region of the source) in the source spectral parameterization. However the use of the Cash statistic has a major disadvantage in that it does not provide a goodness-of-fit criterion for comparing different models: therefore in order to establish the best fit model for a source we apply the χ^2 statistic with the Gehrels weighting method and the F-test. The spectral analysis is carried out using XSPEC v11.0. In computing fluxes and luminosities of our sources, we apply an encircled energy correction factor in order to take into account the *EPIC* energy encircled fraction (Ghizzardi 2001). All luminosities are calculated with $H_0 = 50$ km s^{-1} Mpc^{-1} and $q_0 = 0$. Throughout the paper, errors are given at the 90% confidence level for one interesting parameter ($\Delta\chi^2 = 2.71$; Avni 1976).

3. Results

3.1. Optical and radio properties of the sample

As reported in Table 2, 21 of our 41 X-ray sources (∼50% of the sample) are already optically identified: 9 from the literature, 4 from the *XMM-Newton* International Survey program (*AXIS*, Barcons et al. 2002) and 10 from Fiore et al. (in preparation, hereafter F02). Of these, the majority (15) are broad line AGNs, 2 are narrow emission line galaxies (NELGs), 1 is a Seyfert 2 galaxy, 2 are normal galaxies and one is a red quasar. Source No. 41 has two possible optical counterparts, both of which are normal elliptical galaxies at $z = 0.251$ and $z = 0.254$, respectively (F02). The redshift distribution of these optically identified sources is shown in Fig. 1.

Source No. 3 (CXOU J031238.9−765134) was first discovered by *Chandra* and identified with a bulge dominated normal galaxy without strong optical emission lines at $z = 0.158$ (called "P3" in Fiore et al. 2000). Combined with its high X-ray luminosity, this makes it a classic example of an "optically dull

Table 2. List of the 41 X-ray serendipitous sources included in our sample.

N	Source name	RA (J2000)	Declination (J2000)	z	Classification
		PKS 0312-770 field			
1	CXOU J031015.9−765131	03 10 15.3	−76 51 32	1.187	BL AGN[a]
2	CXOU J031209.2−765213	03 12 08.7	−76 52 11	0.89	BL AGN[a]
3	CXOU J031238.9−765134	03 12 38.8	−76 51 31	0.159	Galaxy[a]
4	CXOU J031253.8−765415	03 12 53.5	−76 54 13	0.683	Red QSO[a]
5	CXOU J031312.1−765431	03 13 11.5	−76 54 28	1.124	BL AGN[a]
6	CXOU J031314.5−765557	03 13 14.2	−76 55 54	0.42	BL AGN[a]
7	XMMU J030911.9−765824	03 09 11.6	−76 58 24	0.268	Sey 2[b]
8	XMMU J031049.6−763901	03 10 49.5	−76 39 01	0.380	BL AGN[b]
9	XMMU J031105.1−765156	03 11 05.1	−76 51 56	–	No cl.
		MS1229.2+6430 field			
10	XMMU J123110.6+641851	12 31 10.6	+64 18 51	–	No cl.
11	XMMU J123116.3+641114	12 31 16.3	+64 11 14	–	No cl.
12	XMMU J123218.6+640309	12 32 18.6	+64 03 09	–	No cl.
13	XMMU J123214.2+640459	12 32 14.2	+64 04 59	–	No cl.
14	XMMU J123013.4+642505	12 30 13.4	+64 25 05	–	No cl.
15	XMMU J123049.9+640845	12 30 49.9	+64 08 45	–	No cl.
16	XMMU J123058.5+641726	12 30 58.5	+64 17 26	–	No cl.
		IRAS13349+2438 field			
17	XMMU J133730.8+242305	13 37 30.8	+24 23 05	–	No cl.
18	XMMU J133649.3+242004	13 36 49.3	+24 20 04	–	No cl.
19	XMMU J133807.4+242411	13 38 07.4	+24 24 11	–	No cl.
20	XMMU J133747.4+242728	13 37 47.4	+24 27 28	–	No cl.
21	XMMU J133712.6+243252	13 37 12.6	+24 32 52	–	No cl.
		Abell 2690 field			
22	XMMU J000031.7−255459	00 00 31.7	−25 54 59	0.283	BL AGN[b]
23	XMMU J000122.8−250019	00 01 22.8	−25 00 19	0.968	BL AGN[b]
24	XMMU J000027.7−250441	00 00 27.7	−25 04 41	0.335	BL AGN[b]
25	XMMU J000100.0−250459	00 01 00.0	−25 04 59	0.851	BL AGN[b]
26	XMMU J000102.5−245847	00 01 02.5	−24 58 47	0.433	BL AGN[b]
27	XMMU J000106.8−250845	00 01 06.8	−25 08 45	–	–
		MS 0737.9+744 field			
28	1E0737.0+7436	07 43 12.5	+74 29 35	0.332	BL AGN[c]
29	XMMU J074350.5+743839	07 43 50.5	+74 38 39	–	No cl.
30	1SAX J0741.9+7427	07 42 02.2	+74 26 24	–	No cl.
31	XMMU J074351.5+744257	07 43 51.5	+74 42 57	–	No cl.
32	XMMU J074401.5+743041	07 44 01.5	+74 30 41	–	No cl.
		Markarian 205 field			
33	MS 1219.9+7542	12 22 06.6	+75 26 14	0.238	NELG[d]
34	MS 1218.6+7522	12 20 52.0	+75 05 29	0.646	BL AGN[d]
35	XMMU J122258.3+751934	12 22 58.3	+75 19 34	0.257	NELG[d]
36	XMMU J122351.3+752224	12 23 51.3	+75 22 24	0.565	BL AGN[d]
37	NGC 4291	12 20 15.9	+75 22 09	0.0058	Galaxy[d]
		Abell 1835 field			
38	XMMU J140127.7+025603	14 01 27.7	+02 56 03	0.265	BL AGN[b]
39	XMMU J140053.0+030103	14 00 53.0	+03 01 03	0.573	BL AGN[b]
40	XMMU J140130.7+024529	14 01 30.7	+02 45 29	–	No cl.
41	XMMU J140145.0+025330	14 01 45.0	+02 53 30	–[†]	Gal.[b,†]

Optical classifications and redshifts are from: [a] Fiore et al. (2000), [b] Fiore et al. 2002 (F02; in prep.), [c] Wei et al. (1999) and [d] AXIS (Barcons et al. 2002). [†] There are two possible candidates for the identification of this source: an elliptical galaxy at $z = 0.251$ or an elliptical galaxy at $z = 0.254$ (F02).

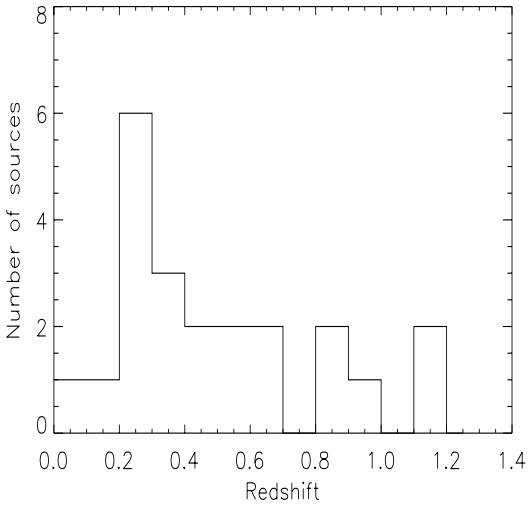

Fig. 1. Redshift distribution of the 21 optically identified sources in the sample. The plotted values range from 0.0058 to 1.187. The average redshift is $\langle z \rangle \sim 0.5$.

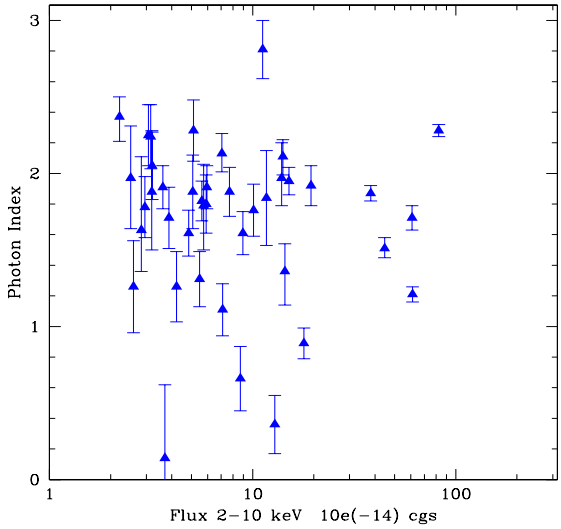

Fig. 2. Broad-band (0.3–10 keV) photon indices obtained using a power law plus Galactic absorption (SPL) model versus 2–10 keV flux for each source in our sample.

X-ray loud" galaxy (Elvis et al. 1981). In the optical image the galaxy appears to be extended with the *Chandra* source centered on its nucleus. Source No. 33 (MS 1219.9+7542) was detected for the first time by the *Einstein* observatory (Gioia et al. 1990), and was first optically identified with a cluster of galaxies by Stocke et al. (1991) in the *EMSS* survey. Subsequently, Rector et al. (2000) classified MS 1219.9+7542 as a BL Lac object on the basis of its spectral energy distribution (SED). Very recently, however, Barcons et al. (2002) unambiguously classified MS 1219.9+7542 as a narrow emission line galaxy (NELG) on the basis of an observation performed with the 2.5 m INT telescope. Source No. 37 (NGC 4291) is an early-type (E2) absorption line galaxy at redshift $z = 0.0058$ (Ho et al. 1997), which is also weakly detected in a 8.5 GHz NRAO VLA observation ($P_{8.5\,\mathrm{GHz}} < 6.3 \times 10^{18}$ W Hz^{-1}, Wrobel & Herrnstein 2000). Stellar dynamical measurements indicate that NGC 4291 has a massive central black hole of 1.8×10^8 solar masses (Gebhardt et al. 2000). This nearby galaxy appears extended in the *EPIC* image. The centroid of the hard X-ray source (α(J2000) = $12^{\mathrm{h}}20^{\mathrm{m}}15^{\mathrm{s}}$, δ(J2000) = $75°22'09''$) is displaced by ∼9 arcsec from the optical center of the galaxy (α(J2000) = $12^{\mathrm{h}}20^{\mathrm{m}}17^{\mathrm{s}}$, δ(J2000) = $75°22'18''$). This value is larger than the *XMM* astrometric errorbox (6 arcsec): the X-ray source is however well inside the optical contour of NGC 4291. We choose a 30 arcsec extraction radius in order to avoid contamination from the nearby X-ray source 1AX J122024+7521 (Ueda et al. 2001) and the previously unknown X-ray source XMMU J122005.1+752143, which are at 55 and 49 arcsec from NGC 4291, respectively.

Finally, the sample is cross-correlated with the FIRST (Becker et al. 1995) and the NVSS (Condon et al. 1998) radio catalogs in order to identify any possible radio counterparts. Only 2 out of 7 fields analyzed here have been covered by the FIRST survey while the NVSS covers all but one fields (PKS 0312-770) but with a higher flux limit. We find that only three X-ray sources have a radio counterpart: sources No. 23, 25 and 38 coincide (within a few arcsec) with the radio sources NVSS 000122.7−250018.6 ($S_{1.4\,\mathrm{GHz}} = 69.2$ mJy), NVSS J000100−250503 ($S_{1.4\,\mathrm{GHz}} = 130$ mJy) and FIRST 140127.59+025606.8 ($S_{1.4\,\mathrm{GHz}} = 1.54$ mJy), respectively. All these sources have optical-to-radio indices $\alpha_{\mathrm{ro}} \geq 0.3$ and can therefore be classified as radio loud AGNs.

3.2. X-ray spectral properties

3.2.1. Single power law model (SPL)

In order to understand the shape of the continuum, the spectrum of each source is first fitted with a simple model consisting of a power law with absorption fixed at the Galactic value (hereafter, model SPL). The results of these fits are reported in Table 3 and graphically displayed in Fig. 2 where we plot Γ versus 2–10 keV flux. The resulting photon indices range from 0.15 to 2.8, with the majority of the sources clustering at around 1.9, i.e. close to the canonical value for broad line unabsorbed AGNs. One source in Fig. 2 is compatible with an inverted (negative) spectral slope and another has $\Gamma \sim 3$. These extreme cases will be discussed in detail in the next Sections. The results obtained by applying the Cash statistic are fully consistent with those obtained using the χ^2 (see Table 3). We also check out the possible presence of systematic variations (i.e. hardening or softening) of the photon index with the off-axis distance of the sources but we find no particular trend. Possible artifacts of the PSF emerging at large radii have been also rejected by Bocchino et al. (2001) after a detailed *MOS* and *PN* spectral analysis of 3C 58. Interestingly enough, it appears from Fig. 2 that very flat Γ ($\leq$1.1–1.2) are present at different flux levels and no trend of Γ versus flux is evident in the data.

3.2.2. Absorbed power law model (APL)

A flat photon index could indicate that the simple power law model is not appropriate. In fact, typically flat X-ray spectra are obtained when absorption intrinsic to the source is present.

Table 3. Fits with a single power law model with Galactic absorption (model SPL).

N	Source name	$N_{\rm H}^{\rm Gal}{}^{a}$ (10^{20} cm^{-2})	Γ^{b}	χ^2_ν/(d.o.f.)	Best−fit
1	CXOU J031015.9−765131	8	$1.87^{+0.05}_{-0.05}$	0.90/250	Yes
2	CXOU J031209.2−765213	8	$2.24^{+0.21}_{-0.21}$	0.91/52	Yes
3	CXOU J031238.9−765134	8	$1.03^{+0.52}_{-0.52}/(1.26^{+0.30}_{-0.30})$	0.69/11	No
4	CXOU J031253.8−765415	8	$1.61^{+0.14}_{-0.14}$	1.02/39	Yes
5	CXOU J031312.1−765431	8	$1.88^{+0.16}_{-0.16}$	1.22/48	Yes
6	CXOU J031314.5−765557	8	$1.95^{+0.09}_{-0.09}$	0.79/81	Yes
7	XMMU J030911.9−765824	8	$0.15^{+0.30}_{-0.41}/(0.36^{+0.19}_{-0.19})$	1.28/28	No
8	XMMU J031049.6−763901	8	$1.36^{+0.18}_{-0.22}$	1.07/35	Yes
9	XMMU J031105.1−765156	8	$1.32^{+0.76}_{-0.61}/(1.88^{+0.41}_{-0.38})$	0.81/11	Yes
10	XMMU J123110.6+641851	2	$1.91^{+0.14}_{-0.14}$	0.76/37	Yes
11	XMMU J123116.3+641114	2	$1.82^{+0.13}_{-0.12}$	1.00/52	Yes
12	XMMU J123218.6+640309	2	$1.88^{+0.24}_{-0.24}$	0.71/24	Yes
13	XMMU J123214.2+640459	2	$1.40^{+0.30}_{-0.30}/(1.31^{+0.18}_{-0.18})$	0.92/24	Yes
14	XMMU J123013.4+642505	2	$1.79^{+0.27}_{-0.29}$	1.14/22	Yes
15	XMMU J123049.9+640845	2	$2.37^{+0.13}_{-0.16}$	1.05/31	Yes
16	XMMU J123058.5+641726	2	$1.08^{+0.34}_{-0.34}/(1.26^{+0.23}_{-0.23})$	0.32/9	Yes
17	XMMU J133730.8+242305	1.2	$2.25^{+0.21}_{-0.21}$	0.58/24	Yes
18	XMMU J133649.3+242004	1.2	$2.05^{+0.22}_{-0.22}$	0.94/24	Yes
19	XMMU J133807.4+242411	1.2	$2.13^{+0.11}_{-0.12}$	1.21/72	No
20	XMMU J133747.4+242728	1.2	$1.92^{+0.34}_{-0.33}$	0.80/24	Yes
21	XMMU J133712.6+243252	1.2	$1.66^{+0.43}_{-0.28}$	1.46/17	Yes
22	XMMU J000031.7−255459	2	$2.13^{+0.13}_{-0.12}$	0.91/19	Yes
23	XMMU J000122.8−250019	2	$1.97^{+0.23}_{-0.18}$	1.11/31	Yes
24	XMMU J000027.7−250441	2	$1.91^{+0.14}_{-0.14}$	0.99/46	Yes
25	XMMU J000100.0−250459	2	$0.89^{+0.10}_{-0.10}$	1.44/28	No
26	XMMU J000102.5−245847	2	$2.28^{+0.20}_{-0.20}$	0.85/52	Yes
27	XMMU J000106.8−250845	2	$1.61^{+0.39}_{-0.33}/(1.71^{+0.20}_{-0.20})$	0.64/19	Yes
28	1E 0737.0+7436	3.5	$2.28^{+0.04}_{-0.04}$	1.05/227	No
29	XMMUJ074350.5+743839	3.5	$1.08^{+0.25}_{-0.25}/(1.11^{+0.17}_{-0.17})$	1.11/13	No
30	1SAX J0741.9+7427	3.5	$1.92^{+0.13}_{-0.13}$	1.11/64	Yes
31	XMMUJ074351.5+744257	3.5	$1.84^{+0.31}_{-0.31}$	0.97/29	Yes
32	XMMUJ074401.5+743041	3.5	$1.71^{+0.34}_{-0.30}/(1.78^{+0.20}_{-0.20})$	0.59/11	Yes
33	MS 1219.9+7542	3	$1.51^{+0.07}_{-0.06}$	0.86/87	No
34	MS 1218.6+7522	3	$1.71^{+0.08}_{-0.08}$	0.69/100	Yes
35	XMMU J122258.3+751934	3	$1.41^{+0.27}_{-0.33}/(1.61^{+0.15}_{-0.15})$	0.93/18	Yes
36	XMMU J122351.3+752224	3	$1.76^{+0.17}_{-0.17}$	0.84/31	Yes
37	NGC 4291	3	$2.81^{+0.19}_{-0.19}$	5.26/72	No
38	XMMU J140127.7+025603	2.3	$1.21^{+0.05}_{-0.05}$	1.55/215	No
39	XMMU J140053.0+030103	2.3	$1.80^{+0.19}_{-0.19}$	0.90/37	Yes
40	XMMU J140130.7+024529	2.3	$0.19^{+0.52}_{-0.62}/(0.14^{+0.48}_{-0.28})$	0.87/7	No
41	XMMU J140145.0+025330	2.3	$0.76^{+0.35}_{-0.35}/(0.66^{+0.21}_{-0.21})$	0.85/19	Yes

[a] Galactic column density are taken from Stark et al. (1992). [b] The values reported in brackets are obtained using the C statistic (Cash 1979), see text for details.

We have therefore refitted our data using a power law but absorbed this time both by Galactic and intrinsic absorption (model APL). Table 4 lists all sources (8 out of 41) for which there is evidence of excess absorption on the basis of a χ^2 improvement in the fit. In source No. 3 the fit improvement is not so significant (at >90%) but the slope is steeper ($\Gamma \sim 1.84$) than without absorption ($\Gamma \sim 1.03$). In source No. 7, the fit improves only slightly but this source clearly requires

Table 4. Fits with a single power law model with extra absorption component (model APL).

Source No.	Γ^a	$N_{\rm H}{}^a$ (10^{21} cm^{-2})	$F-$statistic	C.l.	Best-fit
3	$1.84^{+1.95}_{-1.10}/(2.12^{+0.68}_{-0.24})$	$7.1^{+18.0}_{-7.1}/(11.8^{+5.7}_{-5.7})$	3.1	90.0%	Yes
7	$1.20^{+1.26}_{-1.05}/(1.39^{+0.53}_{-0.53})$	$48.5^{+70.3}_{-48.5}/(37.6^{+26.8}_{-18.5})$	1.14	80.0%	No
25	$1.31^{+0.20}_{-0.19}$	$5.2^{+3.0}_{-2.2}$	18.0	99.99%	Yes
29	$1.75^{+0.72}_{-0.47}/(1.59^{+0.30}_{-0.30})$	$2.7^{+2.8}_{-1.8}/(2.1^{+1.8}_{-0.9})$	7.9	98.5%	Yes
33	$1.64^{+0.09}_{-0.09}$	$0.59^{+0.23}_{-0.23}$	4.8	97.0%	Yes
37	>8.69	$10.7^{+0.5}_{-1.7}$	65.1	>99.99%	No
38	$1.66^{+0.09}_{-0.09}$	$1.5^{+0.2}_{-0.2}$	98	>99.99%	No
40	$2.15^{+3.37}_{-1.84}/(1.74^{+2.75}_{-0.47})$	$23.5^{+120.8}_{-18.5}/(18.1^{+10.4}_{-5.90})$	6.1	96.0%	Yes

[a] The values reported in brackets are obtained using the C statistics (Cash 1979), see text for details.

an additional soft component (see Sect. 3.2.3). In all other sources (Nos. 25, 29, 33, 37, 38 and 41) the improvement is highly significant (at >97%).

In any case it is evident from Table 4 that the power laws steepen to more standard Γ values in most objects, while the column densities obtained range from ~6 to ~200×10^{20} cm^{-2}, i.e. a very broad range of values: in source No. 37 Γ is intrinsically steep but this is due to the peculiar spectral shape of this source (see Sect. 3.2.3).

As expected the only known Seyfert 2 (No. 7) present in the sample is the source with the largest value of $N_{\rm H}$. Note however that other objects characterized by narrow lines (Nos. 4, 33, 35), and so potentially obscured, show very low column density values. Furthermore, although not yet optically classified, XMMU J140130.7+024529 (No. 40) is very likely associated with a type 2 object just on the basis of the column density result obtained here. Significant absorption is also found in two broad line AGNs (Nos. 25 and 38), indicating that also this type of object can contain large amounts of gas; furthermore 2 out of 3 radio loud sources in our sample are obscured in X-rays. Even more interesting is the presence of absorption in two out of three normal galaxies of the sample. Under the assumption that the dust to gas ratio in these objects is similar to our own Galaxy, the observed column densities imply an optical extinction $A_{\rm V} \sim$ 1–2 mag, not high enough to obscure the broad line region of an AGN, and so confirming their optical classification as normal galaxies. Finally source No. 41 does not require any additional absorption component and its spectrum appears to be intrinsically flat ($\Gamma \sim 0.7$). We have also tried imposing a Γ = 1.9, resulting in a column density $N_{\rm H} = 1.1^{+1.2}_{-0.7} \times 10^{22}$ cm^{-2} but this fit is worse than that found with the SPL model. However the lack of optical identification for about half of the sources in the sample and the poor statistics characterizing some faint sources could lead to an artificial underestimate of $N_{\rm H}$. In fact, it is worth noting that some sources with flat best-fit slopes ($\Gamma <$ 1.5) could be obscured by large absorption columns but the low statistics may prevent us from making a correct measurement of the true absorption column density. We have faced both these problems by imposing a photon index of Γ = 1.9 to all sources and z = 1 to optically unidentified objects, before re-estimating the $N_{\rm H}$ values. Results of this spectral fitting will be discussed in Sect. 4.2.2.

3.2.3. More complex models

After the introduction of models SPL and APL four sources (Nos. 7, 19, 28, 37) are still not satisfactorily fitted; in fact the residuals show (see Figs. 3–6) that the presence of a soft excess is these objects is evident. We have therefore refitted these sources introducing an extra spectral component in the form of a power law (PL in Table 4) or a thermal model (TM in Table 4) in addition to the primary power law continuum. The photon index of the secondary power law is left free to vary in all sources whereas in source No. 7 it is fixed to the value of the primary power law photon index as expected in a type 2 object where the soft excess is often due to a scattered component (Turner et al. 1997). The thermal model is parameterized by Raymond-Smith plasma.

Source No. 19 is not optically classified and the introduction of a thermal component is dictated by the high value of the secondary power law photon index ($\Gamma = 5.17^{+1.64}_{-0.43}$). In source No. 28, a double power law model is a good fit to the data and the change in slope is located at $1.30^{+0.31}_{-0.20}$ keV. Many radio-quiet QSOs, as source No. 28 has been optically classified, show such an excess in the soft X-ray band (Reeves & Turner 2000; George et al. 2000; Mineo et al. 2000). This excess is likely due to the high energy tail of the UV bump and is often parameterized by a blackbody component. In fact using such a component in place of the second power law gives an equally good fit (at >99% confidence level with respect to model SPL) and provides a $\Gamma = 1.96^{+0.10}_{-0.09}$ and a $kT = 0.13^{+0.02}_{-0.02}$ keV in the quasar rest frame.

Source No. 37 (NGC 4291) is a normal galaxy and so a thermal component is expected: for the X-ray emitting gas we infer a rather low temperature ($kT \sim 0.4$ keV) and metallicity $Z/Z_{\odot} = 0.07^{+0.04}_{-0.02}$. The introduction of the soft component solves the problem of the rather steep spectral slope but reveals the presence of a hard tail in this object (e.g. Fig. 7). A similar feature has also been found in other X-ray early-type galaxies (Allen et al. 2000; Matsumoto et al. 1997) and is possibly due

Table 5. Fits with an absorbed/unabsorbed power law plus soft thermal (TM)/power law (PL) component model.

Source No.	Model	$\Gamma_{\rm soft}/kT$ (eV)	$N_{\rm H}$ (10^{21} cm^{-2})	$\Gamma_{\rm hard}$	$F-$statistic	C.l.	Best-fit
7	PL	$\equiv \Gamma_{\rm hard}$	$94^{+92}_{-92}/(98^{+41}_{-33})^a$	$1.76^{+0.50}_{-1.17}/(2.17^{+0.48}_{-0.29})^a$	4.4	96%	Yes
19	TM	150^{+50}_{-110}	$\equiv N_{\rm H}^{\rm Gal}$	$1.74^{+0.23}_{-0.19}$	8.1	>99%	Yes
28	PL	$2.47^{+0.08}_{-0.07}$	$\equiv N_{\rm H}^{\rm Gal}$	$1.93^{+0.10}_{-0.10}$	23.5	> 99%	Yes
37	TM	360^{+50}_{-20}	$2.3^{+1.1}_{-0.8}$	$1.11^{+0.50}_{-0.48}$	96.7	>99.99%	Yes

[a] The values reported in brackets are obtained using the C statistic (Cash 1979), see text for details.

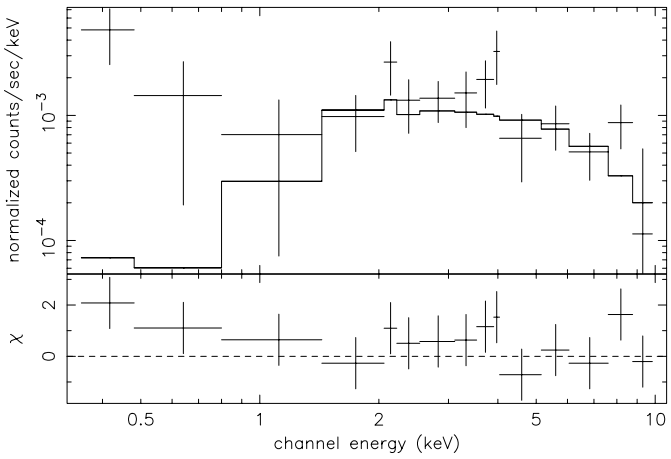

Fig. 3. The *PN* spectrum of XMMU J030911.9-765824 (No. 7) (*upper panel*) fitted with a power law modified by an extra X-ray absorption component (model APL, see Table 4). The residuals of the fit are also shown (*lower panel*). Note the excess in the soft portion of the spectrum.

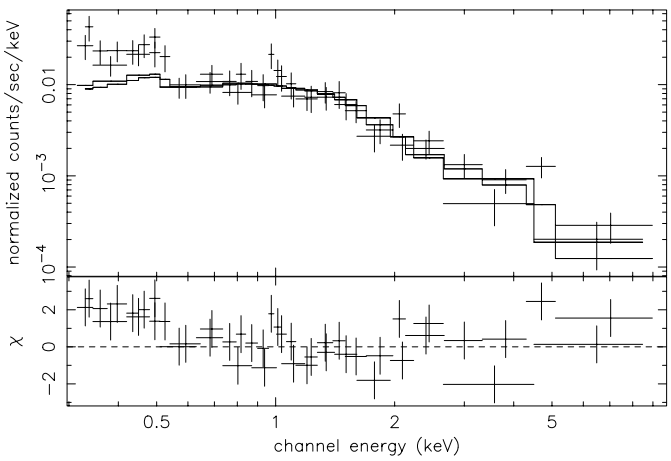

Fig. 4. *MOS1+MOS2* spectra of the unidentified source XMMU J133807+242411 (No. 19) fitted by a simple power law plus Galactic absorption model (*upper panel*). The residuals (*lower panel*) show evidence of a soft excess emission component.

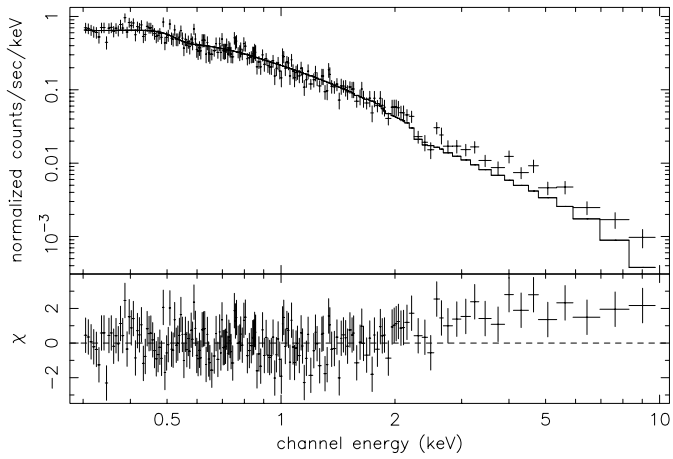

Fig. 5. The *PN* spectrum (*upper panel*) and residuals (*lower panel*) of the broad line QSO 1E 0737.0+7436 (No. 28) when fitted by a simple power law plus Galactic absorption (SPL) model (Table 3).

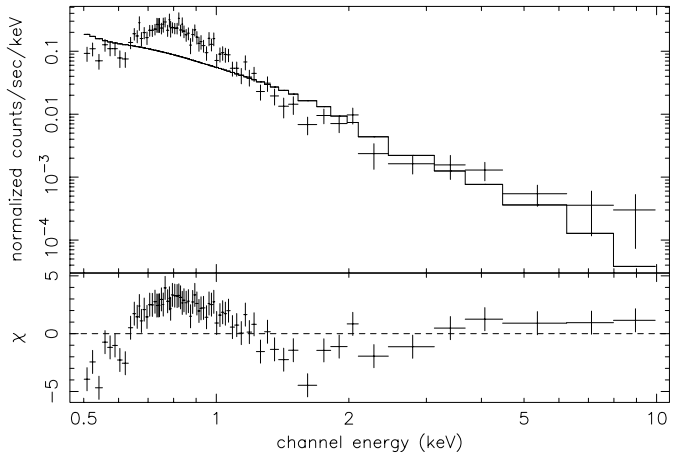

Fig. 6. The *EPIC PN* spectrum of NGC 4291 (No. 37) fitted by a power law (*upper panel*) and relative residuals (*lower panel*). The large residuals indicate that this model is inadequate to describe the present data (Table 3).

either to the presence of an obscured nucleus or to the summed contributions of discrete X-ray sources in the galaxy. If we impose a slope of 1.9 to the power law component likely associated with the nucleus, we obtain a column density of $41^{+30}_{-21} \times 10^{21}$ cm^{-2}, thus invoking an obscured nucleus could be a viable explanation for the hard tail. However, using this model we find $L_{2-10} = 1.7 \times 10^{40}$ erg s^{-1} which provides an $L_{\rm X}/L_{\rm Eddington}$ ratio $\sim 4 \times 10^{-6}$, too low for a normal AGN. Recent *Chandra* results (Sarazin et al. 2001; Loewenstein et al. 2001) indicate that the bulk of the 2–10 keV emission in a number of early-type galaxies originates from discrete galactic sources like LMXBs, HMXBs and/or galactic BHs (Fabbiano et al. 2001; Foschini et al. 2002) and so it is likely that this contribution is present in NGC 4291 too. Unfortunately we cannot investigate more

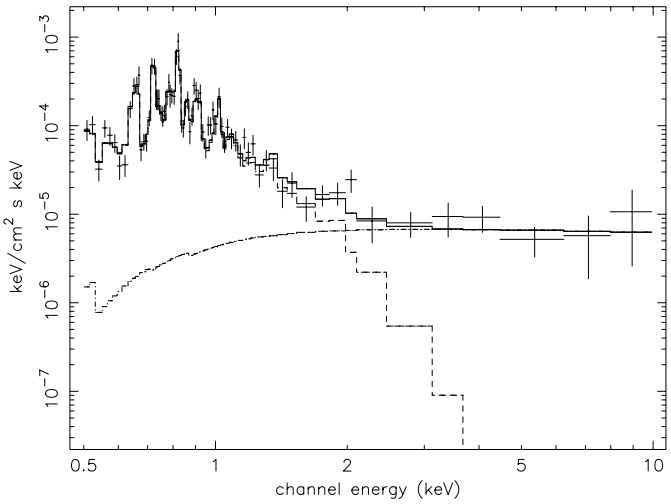

Fig. 7. The *EPIC PN νFν* spectrum of NGC 4291. We also show the two components of the best fit model (see Table 6).

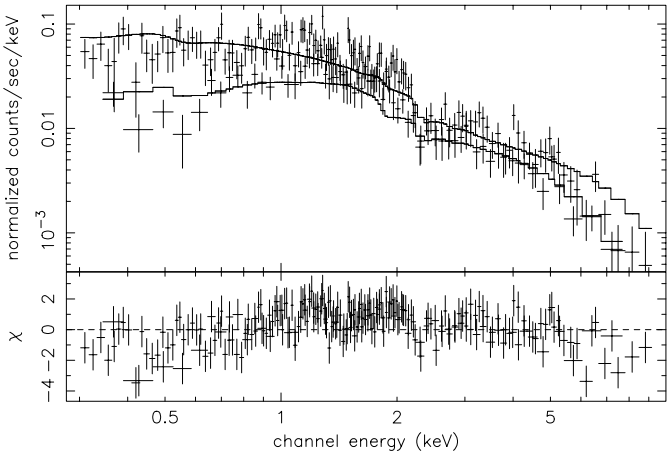

Fig. 8. The *PN+MOS2* spectrum of *XMMU J140127.7+025603.4* fitted with a simple power law (model SPL). Absorption features in the soft as well as in the hard portion of the spectrum are evident.

deeply the origin of the hard X-ray tail because of the limited spatial resolution of *EPIC* with respect to *Chandra* and the low signal to noise ratio at high energies. An observation with higher angular resolution (i.e. with *Chandra*) and longer exposure could instead place stringent limits on the relative contribution of the diffuse gas, discrete sources and a possible hidden low luminosity active nucleus to the total 2–10 keV luminosity of this source.

Finally source No. 38, a broad line radio loud quasar, is characterized by a warm absorber as shown in Fig. 8. In the soft portion of the spectrum we find an edge at 0.82 ± 0.10 keV (quasar-frame) with an optical depth $\tau = 0.42^{+0.15}_{-0.11}$, likely due to OVIII $K-$shell absorption. With this additional component, whose significance is at ∼95% level, the associated $\chi^2(\nu)$ is equal to 218(212). The other edge is found at $E_{\rm abs} = 7.12^{+0.52}_{-0.43}$ keV (quasar-frame) with an optical depth $\tau = 0.71^{+0.46}_{-0.38}$ and a significance >95% confidence level (F-test value = 4.5). This edge is consistent with FeI-XVIII $K-$shell at 90% confidence for $\tau > 0.3$, assuming that the absorbing material is intrinsic to the source. Including this feature in the spectral fitting gives a slightly harder photon index ($\Gamma = 1.55^{+0.05}_{-0.05}$).

We have also checked in the optically identified sources the possible presence of an emission feature centered at 6.4 keV in the source rest frame. No convincing evidence for this line has been found, and in all of the sources considered the upper limits on *EW* we can set are compatible with the values usually observed in active galaxies (≤350 eV).

3.2.4. Summary

About 75% of our sources have not been detected in X-rays before and except for 6 objects (Nos. 1 to 6 in Table 2) in the PKS 0312-770 sky field (for which we find similar results to Lumb et al. 2001), all others have not been spectroscopically studied above 2 keV. 31 out of 41 sources are well fitted with a simple power law plus Galactic absorption (SPL) model (see Table 3). In 7 sources an extra absorption component is required at >95% confidence level (see Tables 4 and 5). Furthermore another source (No. 3 in Table 4) shows a very flat photon index which is indicative of obscuration, but an accurate spectral fitting is limited by the poor statistics. In four sources we find significant soft excess emission, which can be parameterized with a thermal (TM) model in two cases and with a power law (PL) in another case (source No. 7, a Seyfert 2 galaxy) while in one object (No. 28), both the TM and PL models provide an equally good fit. One source (No. 38) is characterized by warm absorber features both in the soft and in the hard portion of its spectrum (indicated as model WA in Table 6). In Table 6 we report the best fit models found for all our of the sources with the corresponding fluxes in the 0.5–2 keV and in the 2–10 keV band as well as the unabsorbed 2–10 keV luminosity. The hard X-ray fluxes range from ∼3 to $\sim 80 \times 10^{-14}$ erg cm^{-2} s^{-1}, with more than 60% of the sources having $F_{2-10} < 10^{-13}$ erg cm^{-2} s^{-1}. The luminosities span from $\sim 2 \times 10^{40}$ to $\sim 5 \times 10^{45}$ erg s^{-1}. Sources with a hard X-ray luminosity $\geq 10^{42}$ erg s^{-1} match well with their optical classification as AGNs, except for the two intriguing "normal" galaxies (Nos. 3 and 41) which are too X-ray bright for their class.

4. Discussion

4.1. Photon index

Using model SPL over the 0.3–10 keV band (see Table 3) we find an average spectral index $\langle\Gamma\rangle = 1.67 \pm 0.04$ (or $\langle\Gamma\rangle = 1.69 \pm 0.04$ if we consider only the subsample consisting of the 27 sources with a 2–10 keV flux brighter than $\sim 5 \times 10^{-14}$ erg cm^{-2} s^{-1}, the value above which we are complete). Using the best fit model (see Table 6) for 40 out of 41 objects[1], the average photon index becomes even steeper ($\langle\Gamma\rangle = 1.74 \pm 0.09$). This value matches well with those typical of broad line quasars as found in previous works (Lawson & Turner 1997; Reeves & Turner 2000) and it is also consistent with the fact that the large majority of our identified sources are

[1] We exclude NGC 4291 (No. 37) because its spectrum is better described by a thermal model (e.g. Table 6) as expected on the basis of its optical classification.

Table 6. *XMM-Newton* properties of the sample. Fluxes and luminosities are obtained using the best fit model listed in Col. 2 for each source of the sample.

Source No.	Best fit Model[†]	$F_{0.5-2}$ (10^{-14} erg cm^{-2} s^{-1})	F_{2-10} (10^{-14} erg cm^{-2} s^{-1})	L_{2-10} (10^{44} erg s^{-1})
1	SPL	22.10	38.1	52.7
2	SPL	4.50	3.15	3.2
3	APL	0.66	2.59	3.5×10^{-2}
4	SPL	3.41	8.95	2.5
5	SPL	4.31	7.70	9.1
6	SPL	10.13	15.14	1.7
7	PL	0.55	12.85	6.8
8	SPL	6.25	14.42	1.3
9	SPL	0.83	3.19	–
10	SPL	2.62	3.61	–
11	SPL	3.60	5.62	–
12	SPL	3.52	5.07	–
13	SPL	1.84	5.48	–
14	SPL	3.51	5.74	–
15	SPL	3.95	2.21	–
16	SPL	0.88	4.22	–
17	SPL	3.86	3.07	–
18	SPL	2.61	3.20	–
19	TM	8.52	14.10	–
20	SPL	1.88	2.51	–
21	SPL	1.43	2.83	–
22	SPL	7.11	7.06	0.3
23	SPL	9.08	13.88	12.2
24	SPL	4.37	5.95	0.4
25	APL	4.10	17.88	7.3
26	SPL	6.40	5.12	0.7
27	SPL	2.10	3.87	–
28	PL	72.32	82.42	5.3
29	APL	2.47	7.11	–
30	SPL	14.41	19.38	–
31	SPL	7.50	11.70	–
32	SPL	1.74	2.95	–
33	APL	18.33	44.6	1.3
34	SPL	30.62	60.93	15.9
35	SPL	1.96	4.84	0.2
36	SPL	6.76	10.11	2.1
37	TM	24.41	11.21	1.7×10^{-4}
38	WA	22.23	61.22	2.2
39	SPL	3.62	5.91	1.3
40	APL	0.31	3.7	–
41	SPL	1.10	8.7	–

[†]SPL = power law model + Galactic absorption; ABL = SPL + additional absorption; TM = SPL (or APL) + thermal model for the soft excess component; PL = SPL (or APL) + non-thermal model for the soft excess component; WA = SPL (or APL) + warm absorber features.

indeed broad line AGNs (see Table 2). Concerning the subsample of sources with $F_{2-10} \geq \sim 5 \times 10^{-14}$ erg cm^{-2} s^{-1}, the average slope we find is fully consistent with the results in Ishisaki et al. (2001) based on the 1–7 keV hardness ratio analysis of 29 hard X-ray selected sources with fluxes $10^{-14} \leq F_{1-7} \leq 10^{-13}$ erg cm^{-2} s^{-1} found in a deep *ASCA* exposure of the Lockman Hole field. Indeed the above authors reported an apparent photon index of $\langle\Gamma\rangle = 1.65 \pm 0.10$. Our value is instead somewhat steeper than that found using the *ASCA LSS* survey ($\langle\Gamma\rangle = 1.51 \pm 0.05$; Ueda et al. 1999)

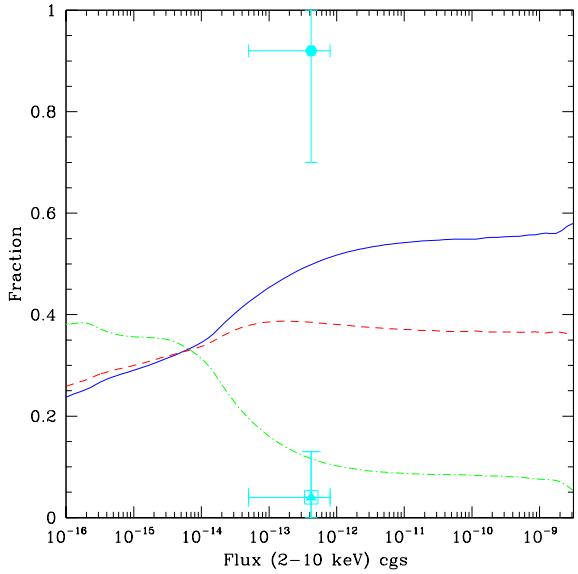

Fig. 9. Fractions of absorbed sources in our complete subsample (*points*) compared to theoretical predictions (*lines*) of Comastri et al. (2001). We use the parameters resulting from the best fit model (Table 6) and, for the optically unidentified sources, $z = 0$. The solid hexagon and the solid line are for $\log N_{\rm H} < 22$ cm^{-2}; the open square and the dashed line are for $22 < \log N_{\rm H} < 23$ cm^{-2}; the solid triangle and the dash-dotted line for $\log N_{\rm H} > 23$ cm^{-2}. Note that the points relative to $22 < \log N_{\rm H} < 23$ cm^{-2} (square) and to $\log N_{\rm H} > 23$ cm^{-2} (triangle) are coincident. The plotted y-error bars correspond to 1σ confidence level according to Gehrels (1986).

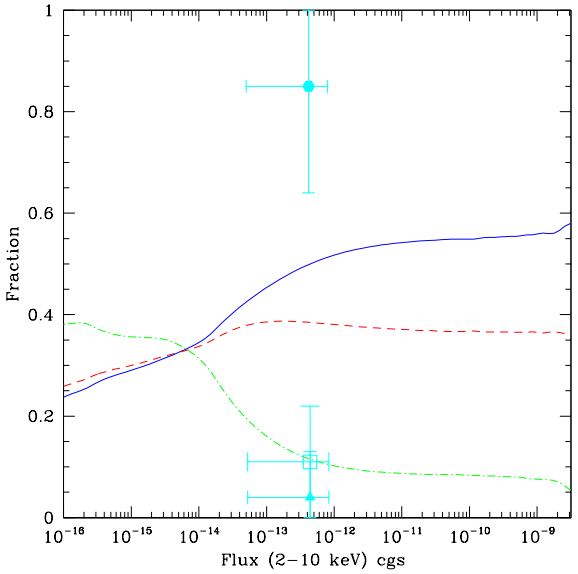

Fig. 10. Fractions of absorbed sources in our complete subsample (*points*) compared to theoretical predictions (*lines*) of Comastri et al. (2001). The difference with Fig. 9 is that, in this case, we force a fit with $\Gamma = 1.9$ for every source and, for the optically unidentified sources in the sample, also we use $z = 1$. Symbols are as in Fig. 9.

obtained from a stacked spectra analysis of 39 X-ray serendipitous sources selected in the 2–10 keV band with $F_{2-10} \geq 8 \times 10^{-14}$ erg cm^{-2} s^{-1}. Ueda et al. (1999) noted however that their result was affected by an artificial spectral flattening due to their hard X-ray selection criterion.

On the other hand, recent *Chandra* and *XMM-Newton* deep surveys indicate that the bulk of sources with flat spectra (intrinsic and/or due to obscuration) which are required to solve the CXB spectral paradox, emerges at 2–10 keV fluxes fainter than 10^{-14} erg cm^{-2} s^{-1}. In fact, our value of $\Gamma \sim 1.6$–1.7 is consistent with the results obtained from the stacked spectra analysis of the *Chandra* Deep Field South (CDFS), where Giacconi et al. (2001) found $\Gamma = 1.71 \pm 0.07$. A progressive hardening of the average slope towards fainter fluxes which is necessary to explain the 2–10 keV CXB spectral shape, has however been measured by Tozzi et al. (2001). Our results are also qualitatively consistent with those recently obtained by Baldi et al. (2002) and Della Ceca et al. (2002) based on a hardness ratio analysis of *XMM-Newton* data where a lack of flat sources above a few 10^{-14} erg cm^{-2} s^{-1} is observed.

Overall, these results match well with the fact that the sources which contribute the most to the hard CXB, lie around the break of the Log N–Log S distribution, i.e. at $F_{2-10} \sim 10^{-14}$ erg cm^{-2} s^{-1}, below which the slope of the Log N–Log S slightly flattens (Cowie et al. 2002; Hasinger et al. 2001; Baldi et al. 2002a). Finally we find no significant correlation between Γ and z for all our optically identified sources.

4.2. Absorption

4.2.1. Broad line X-ray absorbed objects

Interestingly enough we find that ~33% of the sources requiring significant (at 97% confidence level, see Table 4) absorption in excess of the Galactic value are broad line objects with $N_{\rm H}$ ranging from 1 to 5×10^{21} cm^{-2}. Therefore our analysis confirms the existence of broad line AGNs which suffer from absorption in X-rays (Fiore et al. 2001; Georgantopoulos et al. 2001; Schartel et al. 1997; Sambruna et al. 1999) although with lower column densities compared to those found in these works. Also Wilkes et al. (2001) recently reported similar results for a sample of *2MASS* selected AGNs observed by *Chandra*: from the X-ray hardness ratio analysis they found that the majority of type 1 objects are absorbed by intermediate column densities i.e. $N_{\rm H} \sim 10^{21-23}$ cm^{-2}. It is worth stressing that these obscured broad line objects could contribute significantly at progressively fainter fluxes to the fraction of the moderately absorbed sources which produces the bulk of the CXB above 2 keV (see next section).

4.2.2. Comparison with CXB synthesis models

In Fig. 9 we compare the fractions of absorbed sources that we find to the theoretical predictions of the CXB synthesis model of Comastri et al. (2001) relative to the 2–10 keV band. For this plot we consider only sources with $F_{2-10} \geq 5 \times 10^{-14}$ erg cm^{-2} s^{-1} (i.e. our completeness limit). The column densities $N_{\rm H}$ are from the best fit model, as reported in Table 6 for each source. The horizontal error bars associated to the points in Fig. 9 correspond to our completeness limit and to the highest flux in the sample; the vertical error bars indicate instead the Poissonian error for each fraction value.

A mismatch between our findings and the theoretical model predictions is evident from this plot. The latter appear to overestimate by a factor of 2 to 10 the fraction of absorbed sources i.e. with $N_{\rm H} \geq 10^{22}$ cm^{-2}, and understimate the fraction of sources with low absorption. At these flux levels ($F_{2-10} \sim 10^{-13}$ erg cm^{-2} s^{-1}) the model predicts that about 55% of the sources should be obscured, while we find a fraction of 20% at most.

There are, however, some possible biases in our result that should be taken into account. The determination of the true column density for the objects without redshift is difficult and we possibly underestimate some $N_{\rm H}$ values as $N_{\rm H}^{z} \propto (1+z)^{2.6}$ (Barger et al. 2001). To account for this effect as reported in Sect. 3.2.2 we fitted all spectra with an absorbed power law model imposing $\Gamma = 1.9$ (and $z = 1$ for the unidentified sources in the sample) to infer upper limits on the absorption distribution. The results corresponding to these conservative assumptions are reported in Fig. 10. Also in this case we find that the fraction of absorbed sources appears to be lower than the theoretical predicted value, with an upper limit of about 30%.

Another bias we consider important is related to the high energy roll-over of the *PN* effective area above 4 keV. The effective area decreases by about a factor of two between 4 and 9 keV while in order to compute the theoretical predictions showed in Figs. 9 and 10 Comastri et al. (2001) assumed an uniform flat detector response. This fact may have introduced in our analysis a selection bias against the hardest X-ray sources. This problem mostly affects heavily obscured sources with $N_{\rm H} \geq 10^{22-23}$ cm^{-2} which have the bulk of their X-ray emission above 3–4 keV i.e. exactly those sources we do not find in large quantities as foreseen by theoretical models. Because of this bias it is possible that we have lost here some of the faintest, absorbed sources. Spectral analysis of a larger number of sources could help to solve this issue. Note, however, that even if we consider the subsample of sources in the harder 5–10 keV energy band with $F_{5-10} \geq 5 \times 10^{-14}$ erg cm^{-2} s^{-1}, the mismatch between our findings and the theoretical predictions (Comastri et al. 2001) remains. Albeit the number of sources is small (i.e. 15), we notice that our fraction of sources with $N_{\rm H} < 10^{22}$ cm^{-2} is ∼60–80% compared to the Comastri et al. (2001) prediction of ∼35–40%.

We also performed some simulations using *PN* data in order to check the possibility that we missed some absorbed sources (even for those belonging to the "complete" subsample i.e. with $F_{2-10} \geq 5 \times 10^{-14}$ erg cm^{-2} s^{-1}) if their true X-ray spectra are the result of the combination of high column density and scattering of the primary continuum along our line of sight from a warm medium (Turner et al. 1997). To test this hypothesis, we assumed as an input spectrum the average partial covering model (PCF) found in Seyfert 2s (i.e. $\Gamma = 1.96$ and $C_{\rm f} \sim 74\%$; see Turner et al. 1997, Table 19) with a typical flux of 9×10^{-14} erg cm^{-2} s^{-1} in the 0.5–10 keV band (see Table 6). We found that we are able to discriminate at >95% confidence level (using the *F*-test method) between the PCF and APL models for any value of intrinsic $N_{\rm H}$ ranging from 10^{23} down to 10^{21} cm^{-2}. It is worth noting that a column density of $N_{\rm H} = 1 \times 10^{21}$ cm^{-2} at $z = 0$ corresponds to an $N_{\rm H} \leq 10^{22}$ cm^{-2} at $z = 1$. Thus this effect will not change the values plotted in Fig. 10.

Gilli et al. (2001) presented a CXB model which assumes a luminosity density dependent evolution (LDDE; Miyaji et al. 2000) model for the X-ray luminosity function (XLF) and a ratio R absorbed/unabsorbed sources at $z = 0$ ($R = 4$) lower than at $z > 1.32$ ($R = 13$). Comparing our results to their predictions (Gilli, priv. comm.), we confirm a large mismatch for $N_{\rm H} < 10^{22}$ cm^{-2} and $10^{22} < N_{\rm H} < 10^{23}$ cm^{-2}, while for $N_{\rm H} > 10^{23}$ cm^{-2} we are in substantial agreement.

On the other hand some independent recent works based on *Chandra* and *XMM-Newton* observations seem to confirm our results. Gandhi et al. (2001) have carried out a spectroscopic study of serendipitous sources at 2–10 keV fluxes fainter than ours in some *Chandra* cluster observations: they reported that most of these sources are obscured by column densities of $\sim 10^{21-22}$ cm^{-2}, with only a few showing $N_{\rm H} \sim 10^{23}$ cm^{-2}. Preliminary results from the *XMM-Newton* Bright Serendipitous Source Survey discussed in Della Ceca et al. (2002) also report only a few obscured sources at fluxes similar toéours. Finally Baldi et al. (2002b) presented the 2–10 keV hardness ratio distribution of the sources belonging to the *HELLAS2XMM* medium-deep survey. Their sample is larger than ours and also includes all sources presented here (but note their analysis is based only on the hardness ratios rather than spectral fitting). Their results confirm the lack of hard, and hence potentially obscured, sources with hard X-ray fluxes greater than ∼few $\times$ 10^{-14} erg cm^{-2} s^{-1}. For completeness we plot in Fig. 11 the fraction of absorbed objects (i.e. with $N_{\rm H} > 10^{22}$ cm^{-2}) derived from the main X-ray surveys carried out in the 2–10 keV band with different X-ray observatories at different limiting fluxes and the corresponding theoretical model predictions. It appears that at hard X-ray fluxes between 10^{-12} and 10^{-14} erg cm^{-2} s^{-1} the fraction of observed absorbed sources is considerably less than predicted by the theory. This figure clearly shows the inability of CXB standard theoretical models to fit the observational data, at least for fluxes above $F_{2-10} \sim 10^{-14}$ erg cm^{-2} s^{-1}. This result and the mismatch emerging in the optical follow-up of the deep X-ray surveys (Hasinger 2002) between the predicted and the observed redshift distribution of X-ray sources suggests that CXB theoretical models should be revised (Comastri et al., in preparation).

Assuming therefore that the above observational results are real, we address here the possibility of modifying one (or more) of the assumptions made in standard CXB synthesis models. As noted by Gilli et al. (1999), the parameter space of CXB models is large and different combinations of input values can reproduce the CXB properties. The critical assumptions are usually three: the intrinsic X-ray spectral shape of the sources, the XLFs (in particular the XLF of type 1 versus XLF of type 2 objects) and the column density distribution. All these values are already quite uncertain in the local universe and even more importantly their evolution is unknown along z. It is therefore possible that some of the important assumptions used in theoretical models are too rigid. The presence of a steep ($\Gamma > 2$) component in the soft band may not be a ubiquitous feature of low z broad line AGNs (Reynolds 1997; Matt 2000; Reeves & Turner 2000); in particular Blair et al. (2000) suggested

a possible evolution along z of the soft excess in the *ROSAT* spectra of soft X-ray selected QSOs. Furthermore high-z radio quiet QSOs may have flatter intrinsic slopes than nearby ones as found in *ASCA* observations (Vignali et al. 1999; Pappa et al. 2001b).

Another possibility is that QSOs may evolve in luminosity and/or in number differently than assumed in theoretical models. For example Comastri (2000) computed the relative fraction of unobscured and obscured sources assuming a LDDE for the XLF instead of a pure luminosity evolution (PLE; as used in models plotted in Figs. 9 and 10). The model computed in this way predicted a significantly higher number of unobscured sources than expected with a PLE, in better agreement with our observational results. Also recent *Chandra* and *XMM-Newton* deep surveys require modifications to the commonly used XLFs (Hasinger 2002).

The evolution properties of type 2 sources could be different with respect to those of type 1s (see e.g. Gilli et al. 2001). Although the location and the dynamics of the absorption material(s) are two key parameters with which to understand the evolution of type 2 objects, these are only poorly known to date (i.e. Matt 2000b; Guainazzi et al. 2002). For example if the AGNs evolution is connected to the star formation rate in their host galaxies (Oshuga & Umemura 1999) and/or to the growth of the central black hole (Fabian 1999), one might expect a different evolution in the absorption column density of type 1 versus type 2 sources. In particular, a faster evolution of absorbed typeé2 Seyfert-like sources would reduce the above mismatch and would also be consistent with the larger number of flat sources found by e.g. Tozzi et al. (2001) and Baldi et al. (2002b) at lower fluxes than ours.

Finally another possible explanation for the discrepancy between our results and theoretical predictions could be the existence of a new population of sources with flat intrinsic spectra emerging at faint ($\sim 10^{-14}$ erg cm^{-2} s^{-1}) hard X-ray fluxes. In the next Section we discuss possible objects of this kind.

4.3. X-ray loud "normal" galaxies

Two sources in the sample, CXOU J031238.9-765134 (No. 3, the so-called P3 in Fiore et al. 2000; $L_{2-10} \sim 3 \times 10^{42}$ erg s^{-1}) and XMMU J140145.0+025330 (No. 41; $L_{2-10} \sim 2.6 \times 10^{43}$ erg s^{-1} assuming $z = 0.25$), are optically classified as normal galaxies due to the lack of emission lines in their optical spectra, but their hard X-ray luminosities are significantly higher than typically found in the local galaxy population (Fabbiano 1989). For these reasons we consider them as members of the optically dull X-ray bright galaxies class. From our analysis both sources have a flat X-ray photon index with $\Gamma \sim 1$ (No. 3) and $\Gamma \sim 0.7$ (No. 41) when a simple power law model (SPL) is applied. We also derive upper limits on the absorption column density $<10^{23}$ cm^{-2} imposing $\Gamma = 1.9$ in both sources; furthermore, we do not find any evidence of a strong iron line in their spectra, which is a typical features of reflection-dominated objects. Comastri et al. (2002) reported the spectral energy distribution of P3 from radio to X-rays. On the basis of the faintness of its radio emission these authors excluded the presence of an advection dominated accretion flow (Narayan et al. 1998). The SED of P3 could be consistent with a BL Lac-type classification. However the lack of X-ray variability and the presence of a large Calcium break is at odds with such a hypothesis. Based on these overall properties Comastri et al. (2002) suggested that a Compton thick AGN was a very plausible explanation for the X-ray properties of the source. However, the real nature of P3 is still uncertain. Much less is known about source No. 41, so that a detailed investigation on the nature of this object is not possible at the moment.

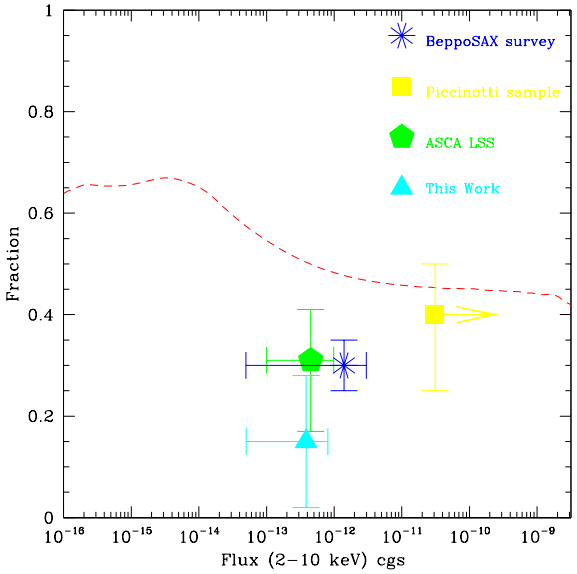

Fig. 11. The fraction of absorbed objects (with $N_{\rm H} > 10^{22}$ cm^{-2}) as reported in the main X-ray surveys carried out in the 2–10 keV band with different X-ray observatories. The dashed line shows the corresponding theoretical fraction of absorbed objects predicted by Comastri et al. (2001). The plotted values are from: Giommi et al. (2000) (*BeppoSAX* survey, *asterisk*); Akiyama et al. (2000) (*ASCA* LSS, *pentagon*); this work (*triangle*). The value for the Piccinotti sample (i.e. 29 AGNs with flux limit of 3×10^{-11} erg cm^{-2} s^{-1}, Piccinotti et al. 1982; *square*) is taken from Comastri (2000). The plotted y-error bars correspond to 1σ confidence level according to Gehrels (1986).

The population of these "normal" galaxies seems to emerge at faint X-ray fluxes, well below 10^{-13} erg cm^{-2} s^{-1}. Such sources have not been found in previous *ASCA* and *BeppoSAX* surveys but this may be due to the large identification error boxes of these observatories. Recently Barger et al. (2001) presented Keck spectroscopy of a complete sample of 20 hard X-ray sources with $F_{2-10} \geq 3.8 \times 10^{-15}$ erg cm^{-2} s^{-1} detected in the *Chandra* Hawaii Deep Survey Field SSA13. Four galaxies in the sample ($\sim$20%) show no clear sign of nuclear activity but have 2–10 keV luminosities greater than 10^{42} erg s^{-1}, i.e. they are X-ray loud. As stated by these authors, these sources may be rather common X-ray emitters. The peculiar characteristics of these sources could be explained by a very high column density obscuring both the broad and narrow line regions of the active nucleus or by beaming. However, as pointed out by Hornschemeier et al. (2001), more accurate optical data are needed before definitively ruling out the possible existence of weak emission lines.

In relation to the CXB population synthesis models, these objects are very interesting because they "appear" at fluxes around 10^{-14} erg cm^{-2} s^{-1} i.e. near the turnover of the Log N–Log S and have a hard photon index. The completion of multiwavelength follow-up observations of pencil beam (Rosati et al. 2002; Hasinger et al. 2001; Willott et al. 2001) and shallower (Baldi et al. 2001; Della Ceca et al. 2002; F02) X-ray surveys will allow an accurate estimate of how common these "normal" galaxies are and what is their relative contribution to the CXB.

5. Conclusions

We have reported spectral results for a sample of 41 hard X-ray sources detected serendipitously in seven *EPIC* fields and selected in the 2–10 keV band. A detailed spectral analysis has been performed in order to measure source-by-source the 0.3–10 keV continuum shape, the amount of cold (and, possibly, ionized) absorbing matter and the strength of other spectral features. Complementary to deep pencil beam surveys, our shallower survey allows us to investigate in some detail the spectral properties of faint serendipitous sources. This is a field of study almost unexplored with previous X-ray satellites. We have found an average photon index $\langle\Gamma\rangle = 1.67 \pm 0.04$ using a simple power law fit with Galactic absorption for the whole sample. Considering only sources with $F_{2-10} \geq 5 \times 10^{-14}$ erg cm^{-2} s^{-1} (i.e. our completeness limit) we obtain a $\langle\Gamma\rangle = 1.69 \pm 0.04$, which is consistent with average values reported in recent *Chandra* and *ASCA* works at similar fluxes.

We have also shown how surveys of the kind described here can constrain some of the assumptions used in CXB population synthesis models (either spectral shape, XLF and/or column density distribution). In particular, we found a mismatch between our observational results and those predicted by the CXB theoretical models relative to the fractions of absorbed versus unabsorbed sources above 5×10^{-14} erg cm^{-2} s^{-1} in the range 2–10 keV. Extremely deep pencil beam exposures do not stress this trend, very likely because of their bias towards fainter fluxes in the source selection. We have also been able to collect information about unusual objects such as broad line X-ray obscured AGNs and optically dull X-ray bright galaxies. We are currently analysing further *XMM-Newton* observations with a goal of obtaining at least 100 source spectra which will allow us to put our results on more sound statistical grounds.

Acknowledgements. We thank the *Hellas2XMM* Team for the optical identifications. We thank Andrea Comastri for providing us some results from his CXB synthesis model in electronic form. We also thank the anonymous referee for his/her suggestions that helped to improve the manuscript considerably. We are grateful to Roberto Gilli, Alessandro Baldi, and Roberto Della Ceca for interesting comments. E.P. thanks Andrea De Luca and Matteo Guainazzi for helpful discussions on data reduction procedure. This research has also made use of the Simbad database, operated by the Centre de Données Astrophysique de Strasbourg (CDS). This work is partially supported by the Italian Space Agency (ASI). E.P. acknowledges financial support from MIUR for the Program of Promotion for Young Scientists P.G.R.99.

References

Akiyama, M., Ohta, K., Yamada, T., et al. 2000, ApJ, 532, 700
Alexander, D. M., Brandt, W. N., Hornschemeier, A. E., et al. 2001, AJ, 122, 2156
Allen, S. W., Di Matteo, T., & Fabian, A. C. 2000, MNRAS, 311, 493
Avni, Y. 1976, ApJ, 210, 642
Baldi, A., Molendi, S., Comastri, A., et al. 2002a, Proc. of New Visions of the Universe in the XMM-Newton and Chandra era, ed. F. Jansen, et al. [astro-ph/0201525]
Baldi, A., Molendi, S., Comastri, A., et al. 2002b, ApJ, 564, 190
Barcons, X., Carrera, F. J., Watson, M. G., et al. 2002, A&A, 382, 522
Barger, A. J., Cowie, L. L., Mushotzky, R. F., & Richards, E. A. 2001, AJ, 121, 662
Becker, R. H., White, R. L., & Helfand, D. J. 1995, ApJ, 450, 559
Blair, A. J., Stewart, G. C., Georgantopoulos, I., et al. 2000, MNRAS, 314, 138
Bocchino, F., Warwick, R. S., Marty, P., et al. 2001, A&A, 369, 1078
Brandt, W. N., Alexander, D. M., Hornschemeier, A. E., et al. 2001a, AJ, 122, 2810
Brandt, W. N., Guainazzi, M., Kaspi, S., et al. 2001b, AJ, 121, 591
Cappi, M., Matsuoka, M., Comastri, A., et al. 1997, ApJ, 478, 492
Cash, W. 1979, ApJ, 228, 939
Collinge, M. J., & Brandt, W. N. 2000, MNRAS, 317, L35
Comastri, A. 2000, Proc. of X-ray Astronomy '99: Stellar Endpoints, AGNs and the Diffuse X-ray Background [astro-ph/0003437]
Comastri, A., Fiore, F., Vignali, C., et al. 2001, MNRAS, 327, 871
Comastri, A., Mignoli, M., Ciliegi, P., et al. 2002, ApJ, in press
Condon, J. J., Cotton, W. D., Greisen, E. W., et al. 1998, AJ, 115, 1693
Cowie, L. L., Barger, A. J., Bautz, M. W., et al. 2001, ApJ, 551, L9
Cowie, L. L., Garmire, G. P., Bautz, M. W., et al. 2002, ApJ, in press [astro-ph/0201186]
Crawford, A. S., Gandhi, P., Fabian, A. C., et al. 2001, MNRAS, in press
DellaCeca, R., Castelli, G., Braito, V., et al. 1999, ApJ, 524, 674
DellaCeca, R., Maccacaro, T., Caccianiga, A., et al. 2002, Proc. of New Visions of the Universe in the XMM-Newton and Chandra era, ed. F. Jansen et al. [astro-ph/0202150]
Elvis, M., Schreier, E. J., Tonry, J., et al. 1981, ApJ, 246, 20
Fabian, A. C. 1999, MNRAS, 308, L39
Fabian, A. C., & Iwasawa, K. 1999, MNRAS, 303, L34
Fabian, A. C., Wilman, R. J., & Crawford, A. S. 2001, MNRAS, in press
Fabbiano, G. 1989, ARA&A, 27, 87
Fabbiano, G., Zezas, A., & Murray, S. S. 2001, ApJ, 554, 1035
Fiore, F., LaFranca, F., Vignali, C., et al. 2000, New Astron., 5, 143
Fiore, F., Comastri, A., LaFranca, F., et al. 2001, Deep Fields ESO Proc. [astro-ph/0102041]
Foschini, L., Di Cocco, G., Dadina, M., et al. 2002, Proc. of New Visions of the Universe in the XMM-Newton and Chandra era, ed. F. Jansen, et al. [astro-ph/0202247]
Gallagher, S. C., Brandt, W. N., Laor, A., et al. 2000, ApJ, 546, 795
Gandhi, P., Crawford, C. S., Fabian, A. C., et al. 2001, Proc. of Galaxy Clusters and the High Redshift Universe Observed in X-rays, ed. D. Neumann, F. Durret, & J. Tran Thanh Van [astro-ph/0106139]
Gebhardt, K., Bender, R., & Bower, G. 2000, ApJ, 539, L13
Georgantopoulos, I., Nandra, K., & Ptak, A. 2001, Proc. of X-ray astronomy 2000 (Palermo Sep. 2000), in press
George, I. M., Turner, T. J., Yaqoob, T., et al. 2000, ApJ, 531, 52
Ghizzardi, S. 2001, XMM-SOC-CAL-TN-0022
Giacconi, R., Rosati, P., Tozzi, P., et al. 2001, ApJ, 551, 624
Gilli, R., Risaliti, G., & Salvati, M. 1999, A&A, 347, 424
Gilli, R., Salvati, M., & Hasinger, G. 2001, A&A, 366, 407

Gioia, I. M., Maccacaro, T., Schild, R. E., et al. 1990, ApJS, 72, 567
Giommi, P., Perri, M., & Fiore, F. 2000, A&A, 362, 799
Gondoin, Ph., Aschenbach, B., Erd, C., et al. 2000, Proc. of SPIE 2000, in press
Guainazzi, M., Matt, G., Fiore, F., & Perola, G. C. 2002, A&A, 388, 787
Halpern, J. P., Turner, T. J., & George, I. M. 1999, MNRAS, 307, L47
Hasinger, G., Altieri, B., Arnaud, M., et al. 2001, A&A, 365, L45
Hasinger, G. 2002, Proc. of New Visions of the Universe in the XMM-Newton and Chandra era, ed. F. Jansen, et al. [astro-ph/0202430]
Ho, L. C., Filippenko, A. V., & Sargent, W. L. N. 1997, ApJ, 487, 568
Hornschemeier, A. E., Brandt, W. N., Garmire, G. P., et al. 2001, ApJ, 554, 742
Jansen, F., Lumb, D. H., Altieri, B., et al. 2001, A&A, 365, L1
LaFranca, F., Fiore, F., Vignali, C., et al. 2000, Proc. of The New Era of Wide Field Astronomy [astro/ph 0011008]
Lawson, A. J., & Turner, M. J. L. 1997, MNRAS, 288, 920
Loewenstein, M., Mushotzky, R. F., Angelini, L., et al. 2001, ApJ, 555, L21
Lumb, D. H., Guainazzi, M., & Gondoin, P. 2001, A&A, 376, 387
Lumb, D. H., Warwick, R. S., Page, M., & De Luca, A. 2002, A&A, 389, L39
Maloney, P. R., & Reynolds, C. S. 2000, ApJ, 545, L23
Marshall, F. E., Boldt, E. A., Holt, S. S., et al. 1980, ApJ, 235, 4
Matsumoto, H., Koyama, K., Awaki, H., et al. 1997, ApJ, 482, 133
Matsushita, K., Ohashi, T., & Makishima, K. 2000, PASJ, 52, 685
Matt, G. 2000a, Proc. of X-ray Astronomy '99: Stellar Endpoints, AGNs and the Diffuse X-ray Background [astro-ph/0007105]
Matt, G. 2000b, A&A, 355, L13
Mineo, T., Fiore, F., Laor, A., et al. 2000, A&A, 359, 471
Miyaji, T., Hasinger, G., & Schmidt, M. 2000, A&A, 353, 25
Narayan, R., Mahadevan, R., & Quataert, E. 1998, The Theory of Black Hole Accretion Discs, ed. A. Abramowicz, G. Bjornsson, & J. E. Pringle (Cambridge: Cambridge University Press) [astro-ph/9803141]
Norman, C., Hasinger, G., Giacconi, R., et al. 2001, ApJ, 571, 218
Ohsuga, K., & Umemura, M. 1999, ApJ, 521, L130
Pappa, A., Georgantopoulos, I., Stewart, G. C., & Zezas, A. L. 2001a, MNRAS, 326, 995
Pappa, A., Stewart, G. C., Georgantopoulos, I., et al. 2001b, MNRAS, 327, 499
Rector, T. A., Stocke, J. T., Perlman, E. S., et al. 2000, AJ, 120, 1626
Reeves, J. N., & Turner, M. J. L. 2000, MNRAS, 316, 234
Reynolds, C. S. 1997, MNRAS, 286, 513
Risaliti, G., Marconi, A., Maiolino, R., et al. 2001, A&A, 371, 37
Rosati, P., Tozzi, P., Giacconi, R., et al. 2002, ApJ, 566, 667
Sakano, M., Koyama, K., Tsuru, T., et al. 1998, ApJ, 505, 129
Salvati, M., & Maiolino, R. 2000, Large Scale Structure in the X-ray Universe, ed. M. Plionis, & I. Georgantopoulos (Paris: Atlantisciences), 277
Sambruna, R. M., Eracleous, M., & Mushotzky, R. F. 1999, ApJ, 526, 60
Sarazin, C. L., Irwin, J. A., & Bregman, J. N. 2001, ApJ, 556, 533
Schartel, N., Schmidt, M., Fink, H. H., et al. 1997, A&A, 320, 696
Stern, D., Moran, E. C., Coil, A. L., et al. 2001, ApJ, in press
Stocke, J. T., Morris, S. l., Gioia, I. M., et al. 1991, ApJS, 76, 813
Struder, L., Briel, U., Dennerl, K., et al. 2001, A&A, 365, L18
Tozzi, P., Rosati, P., Nonino, M., et al. 2001, ApJ, 562, 42
Turner, T. J., George, I. M., Nandra, K., & Mushotzky, R. F. 1997, ApJ, 488, 164
Turner, M. J. L. T., Abbey, A., Arnaud, M., et al. 2001, A&A, 365, L27
Ueda, Y., Takahashi, T., Inoue, H., et al. 1999, ApJ, 518, 656
Ueda, Y., Ishisaki, Y., Takahashi, T., et al. 2001, ApJS, 133, 1
Vecchi, A., Molendi, S., Guainazzi, M., et al. 1999, A&A, 349, L73
Vignali, C., Comastri, A., Cappi, M., et al. 1999, ApJ, 516, 582
Vignali, C., Mignoli, M., Comastri, A., et al. 2000, MNRAS, 314, L11
Wei, J. Y., Xu, D. W., Dong, X. Y., & Hu, J. Y. 1999, A&AS, 139, 575
Wilkes, B. J., Schmidt, G. D., Cutri, R. M., et al. 2001, ApJ, 564, 65
Willott, C. J., Almaini, O., Manners, J., et al. 2001, Proc. of Galaxy Clusters and the High Redshift Universe Observed in X-rays, ed. D. Neumann, F. Durret, & J. Tran Thanh Van [astro-ph/0105560]
Wrobel, J. M., & Herrnstein, J. R. 2000, ApJ, 531, 716
Yaqoob, T. 2000, Large Scale Structure in the X-ray Universe, ed. M. Plionis, & I. Georgantopoulos (Paris: Atlantisciences), 257
Yuan, W., Matsuoka, M., Wang, T., et al. 2000, ApJ, 545, 625